




Vortex laser beam generation from laser interaction with azimuthal plasma phase slab at relativistic intensities

Tianyun Long ^{1,2}, Cangtao Zhou,^{2,*} Sizhong Wu,² Libao Ju ², Ke Jiang ^{2,3}, Ruixue Bai,^{1,2} Taiwu Huang,² Hua Zhang,² Mingyang Yu,² Shuangchen Ruan,² and Xiantu He^{1,2,4,†}

¹*Center for Applied Physics and Technology, HEDPS, and School of Physics, Peking University, Beijing 100871, China*

²*Center for Advanced Material Diagnostic Technology, and College of Engineering Physics, Shenzhen Technology University, Shenzhen 518118, China*

³*Graduate School, China Academy of Engineering Physics, Beijing 100088, China*

⁴*Collaborative Innovation Center of IFSA (CICIFSA), Shanghai Jiao Tong University, Shanghai 200240, China*



(Received 2 August 2020; accepted 25 January 2021; published 8 February 2021)

It is shown theoretically and by simulation that a Gaussian laser beam of relativistic intensity interacting with a uniform-thickness plasma slab of azimuthally varying density can acquire orbital angular momentum (OAM). During the interaction, the laser ponderomotive force and the charge-separation force impose a torque on the plasma particles. The affected laser light and plasma ions gain oppositely directed axial OAM, but the plasma electrons remain almost OAM free. High OAM conversion efficiency is achieved due to the strong azimuthal electromagnetic energy flow during the laser phase modulation. The present scheme should provide useful reference for applications requiring relativistic-intense vortex light.

DOI: [10.1103/PhysRevE.103.023204](https://doi.org/10.1103/PhysRevE.103.023204)

I. INTRODUCTION

Light can carry both spin and orbital angular momentum (OAM) [1–4], corresponding to the light polarization and azimuthal phase structure, respectively. Light with OAM, or vortex light, has applications as optical tweezers [5–7], in quantum entanglement research [8], microscopy [9], nonlinear wave mixing [10], etc. High-power lasers at relativistic intensities with $a_0 \geq 1$ are common nowadays, where $a_0 = eE_0/m_e c \omega$ is the normalized peak laser intensity with m_e and e the electron rest mass and charge, E_0 and ω are the laser electric field amplitude and frequency, and c is the speed of light in vacuum. Applications of vortex light at relativistic intensities have been proposed, such as for positron and electron acceleration [11–13], OAM transfer between light and matter [14], high-order vortex harmonics realization [15,16], generating γ -ray beams with OAM [17,18], etc.

A typical vortex laser beam profile is the Laguerre-Gaussian (LG) envelope structure, which in cylindrical coordinates (r, ϕ, x) is given by

$$\begin{aligned} \text{LG}_{pl} = C_{pl} \frac{w_0}{w} \left(\frac{r\sqrt{2}}{w} \right)^{|l|} \exp\left(\frac{-r^2}{w^2}\right) L_p^{|l|} \left(\frac{2r^2}{w^2} \right) \\ \times \exp(-il\phi) \exp\left(\frac{-ikr^2}{2R}\right) \exp(i\psi), \end{aligned} \quad (1)$$

where C_{pl} is the mode amplitude, w_0 is the beam waist, $w = w_0 \sqrt{1 + (x/x_R)^2}$, $x_R = \pi w_0^2/\lambda$ is the Rayleigh length, $L_p^l(x)$ is the generalized Laguerre polynomial, k is the wave

number, $\psi = (2p + |l| + 1) \arctan(x/x_R)$ is the Gouy phase, and $R = (x^2 + x_R^2)/x$. Thus, p corresponds to the number of radial nodes in the laser intensity, and l is the topological charge, corresponding to OAM of $l\hbar$ per photon on average. Thus LG₀₀ is just the Gaussian structure. For nondestructive conversion of relatively weak Gaussian light into vortex light, methods including the use of holograms [19], spiral phase plates [20], transformation media [21], q plates [22], and nanoscale array [23] are available. However, these methods are not suitable for high-intensity lasers, since the materials used for phase control will be damaged before the conversion completes. Novel methods invoking laser-plasma interaction have been proposed recently for realizing intense vortex light, including the use of light fan [24], plasma hologram [25], and stimulated Raman scattering [26]. However, these new methods might present some restrictions for further OAM-related applications, either for the possible interference by the incident laser(s), or for the complexity resulted from multi-incident beams. Recently we proposed a scheme utilizing an underdense plasma of spiral thickness in generating both single- and multimode relativistic vortex laser light in the transmission direction [27]. Nonetheless, the OAM conversion efficiency in this scheme is, like the other methods, limited to peak around just one third.

In this paper we propose an efficient conceptual scheme for generating vortex light of relativistic intensity by irradiating a uniform-thickness plasma slab having azimuthally varying density with an intense Gaussian laser beam. During the interaction, the plasma modifies the phase of the incident laser beam such that its structure becomes helical. Nearly equal but oppositely directed OAM is generated in the laser light and the plasma ions, but the plasma electrons and the total laser-plasma system remain nearly OAM free. The physics of

*zcangtao@sztu.edu.cn

†xthe@iapcm.ac.cn

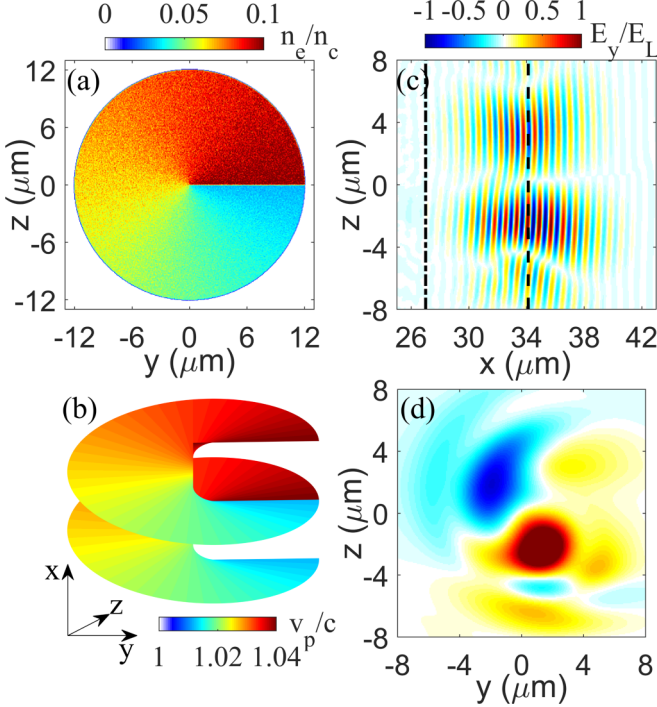


FIG. 1. (a) Transverse electron density profile of the plasma phase plate. (b) Helical phase profile of the $l = 1$ vortex mode. The color code corresponds to the phase velocity. (c) Normalized instantaneous electric field component E_y of the generated vortex laser at $68T_0$ in the x, z plane. The dash-dotted line marks the plasma left boundary. (d) E_y in the transverse plane at $x = 34.1 \mu\text{m}$, marked by the dashed line in (c).

OAM transfer between the laser light and plasma is analyzed in terms of the laser ponderomotive force. Due to the strong azimuthal electromagnetic energy flow, the OAM conversion efficiency in producing the LG_{01} mode can reach as high as 73%. The nonlinear modulation of laser phase velocity resulting from laser energy flow is also discussed and the modulated plasma slab length is given.

II. THEORY AND NUMERICAL SIMULATION

When an intense Gaussian laser pulse irradiates a plasma with azimuthally varying density, as shown in Fig. 1(a), the local laser phase velocity v_p will be modulated azimuthally according to [28] $v_p = c/\sqrt{1 - n_e/\gamma_L n_c}$, where n_e is the plasma density, $n_c = \epsilon_0 m_e \omega^2 / e^2 = 1.7 \times 10^{21} \text{ cm}^{-3}$ the critical density corresponding to laser with wavelength of $0.8 \mu\text{m}$, and $\gamma_L = \sqrt{1 + a_0^2/2}$ is the relativistic factor for linearly polarized (LP) light. With a proper azimuthal plasma density profile, v_p can depend linearly on ϕ like $v_p = (v_1 - v_2)(2\pi - \phi)/(2\pi) + v_2$, with $v_{1,2}$ the maximum and minimum phase velocity, corresponding to the maximum and minimum plasma density $n_{1,2}$, respectively. When the Gaussian laser pulse propagates through such a plasma slab, say of length L , the originally separate plane equiphase surfaces will evolve into a continuous helical surface with azimuthal dependence $\exp(-il\phi)$, together with azimuthally varying v_p . The helical phase structure of the $l = 1$ mode is shown in

Fig. 1(b). Thus, for obtaining a vortex mode with topological charge l , we require $ck(L/v_2 - L/v_1) = 2\pi l$, resulting in

$$L = \frac{v_1 v_2}{v_1 - v_2} \frac{l\lambda}{c}. \quad (2)$$

During the phase modulation, the laser intensity also redistributes due to electromagnetic energy flow [2,27], leading to formation of a singular dark region at the center of the output vortex beam.

The laser plasma interaction is simulated using the fully relativistic particle-in-cell code EPOCH [29]. At $t = 0$, an LP laser with polarization along y direction, $5 \mu\text{m}$ focal radius, $0.8 \mu\text{m}$ wavelength, and Gaussian profile $\exp[-(t - t_0)^2/\Delta t^2]$ is incident along the x axis from the left boundary. Here $t_0 = 10T_0$ and $\Delta t = 5T_0$, T_0 is the laser period. The peak laser intensity is $I_0 = 2.14 \times 10^{18} \text{ W/cm}^2$, or $a_0 = 1$ for the normalized laser amplitude. Simulations show that with a uniform-density plasma of width of tens of micrometers, laser energy dissipation in the plasma remains below several percent for $n_e \leq 0.1n_c$, but abruptly jumps up to tens percent for $n_e > 0.2n_c$. Furthermore, for $n_e \ll n_c$, the relativistic laser ponderomotive force [30] $\vec{f}_p = -m_e c^2 \nabla(1 + a^2/2)^{1/2}$, with $a = eE/m_e c \omega$ and E the laser electric field, can expel almost all the affected electrons, causing local electron cavitation [28], which is also detrimental for controlled laser-phase modulation, where stability is required [31]. For the laser parameters considered here, electron cavitation can be avoided if $n_e > 0.002n_c$. The lightest known solid material is aerographene with density as low as 0.16 kg/m^3 [32], corresponding to a plasma density of several n_c down to $0.028n_c$ with full ionization. Plasma slab with the azimuthally varying density shown in Fig. 1(a) may be fabricated from aerographene using 3D printing [33]. In our simulation, the underdense hydrogen plasma has a counterclockwise decreasing density given by $n_e = (n_1 - n_2)(2\pi - \phi)/(2\pi) + n_2$, i.e., from $n_1 = 0.1n_c$ to $n_2 = 0.03n_c$, as shown in Fig. 1(a). This corresponds to a linear dependance of v_p on ϕ , with $v_1 = 1.0435c$ and $v_2 = 1.0125c$. The plasma length from Eq. (2) should be $L = 27 \mu\text{m}$ for generation of the LG_{01} mode. The simulation box is $-10 < x < 45 \mu\text{m}$ and $-13 < (y, z) < 13 \mu\text{m}$. The cell size is $1/15 \mu\text{m}$ in all directions. The disk plasma is located in $0 < x < L$ and its radius is $12 \mu\text{m}$. There are ten macro particles per cell.

As the Gaussian laser passes through the slab, laser phases are modulated leading to a π shift between the symmetric regions about beam axis, and laser energy redistributes into a hollow structure with nearly null intensity around beam axis, as shown in Figs. 1(c) and 1(d). Mode decomposition of the output laser near plane $x = 34.1 \mu\text{m}$ presents a vortex mode superposition of $0.08\text{LG}_{00} + 0.74e^{i\phi_1}\text{LG}_{01} + 0.19e^{i\phi_2}\text{LG}_{02}$, where $\phi_1 \approx 1.8$ and $\phi_2 \approx 3.8$, with the desired LG_{01} mode dominating indeed.

The process of OAM transfer between laser and plasma is described in Fig. 2. The much lighter electrons gain nearly 3% of the injected laser energy, and the protons gain less than 0.02%. In fact, the protons remain nearly stationary in the process, with maximum velocity about $0.001c$. Figures 2(a) and 2(b) show the electron and proton azimuthal momentum densities P_{ϕ_e} and P_{ϕ_p} , respectively, in the (ϕ, x) plane, at $r = 2 \mu\text{m}$ and $t = 44T_0$, when the pulse center is at

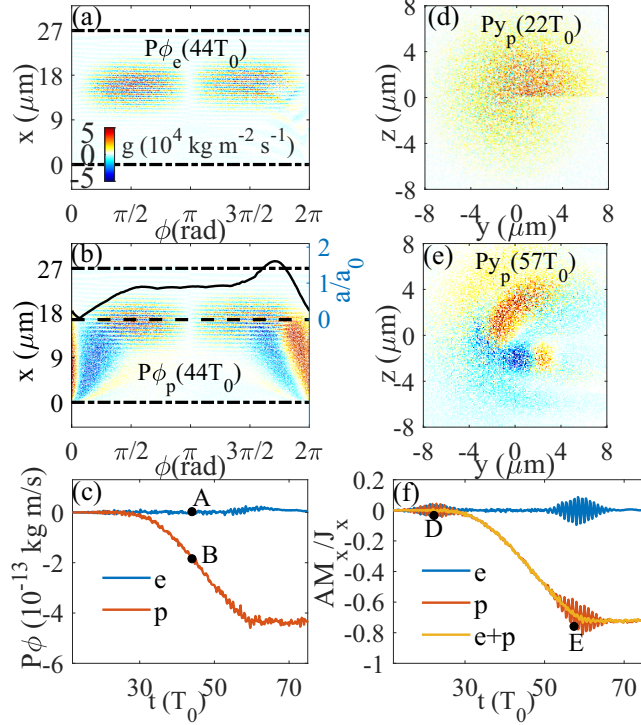


FIG. 2. Azimuthal momentum density distribution in the (ϕ, x) plane at $r = 2 \mu\text{m}$ and $t = 44T_0$ for (a) electrons and (b) protons, for simplicity denoted by P_{ϕ_e} and P_{ϕ_p} , respectively. The dot-dashed lines outline the plasma boundaries. The black curve in (b) shows the normalized laser field intensity a/a_0 at $x = 16.7 \mu\text{m}$ (marked by a dashed line), or the laser-pulse center at $t = 44T_0$. (c) Evolution of the total azimuthal momentum of the electrons (upper curve) and protons (lower curve) in a $0.8 \mu\text{m}$ thick slice centered at $r = 2 \mu\text{m}$. Points A and B correspond to (a) and (b). (d) and (e) Instantaneous y component proton momentum density in the y, z plane at $x = 1.1 \mu\text{m}$ and $t = 22T_0$ and at $x = 25.5 \mu\text{m}$ and $t = 57T_0$, respectively. The color scale in (b), (d), and (e) is the same as that in (a). (f) Evolution of the total normalized axial angular momentum of electrons (upper curve), protons (lower curve with oscillations), and all particles (lower curve without the oscillations). Points D and E correspond to (d) and (e).

$x \sim 16.7 \mu\text{m}$. Around $13 < x < 20 \mu\text{m}$, both P_{ϕ_e} and P_{ϕ_p} oscillate with the laser electric field E_y , with their maxima centered around $\phi = \pi/2$ and $3\pi/2$, but with opposite signs. However, the protons also have a nonoscillating P_{ϕ_p} component in a region behind the pulse center. This phenomenon can be understood as follows. During the phase modulation process, laser energy flows [27] from $\phi \sim 0^+$ to $\sim 2\pi^-$, accompanied by radial energy flow, resulting in a nonuniform averaged azimuthal electric field intensity distribution, as shown by the black curve in Fig. 2(b). The field gradient produces an intense azimuthal ponderomotive force that displaces the local electrons. The resulting azimuthal charge-separation force acting on the protons leads to azimuthal proton momentum gain. Due to the plasma density variation along ϕ , protons in the higher density region $\phi < \pi/2$ will have larger negative azimuthal momentum than that with positive azimuthal momentum in the low density region $\phi > 3\pi/2$. The evolution of the total electron and proton azimuthal momentum in a

$0.8 \mu\text{m}$ thick slice centered at $r = 2 \mu\text{m}$ is shown in Fig. 2(c). We see that the fast oscillating P_{ϕ_e} results in almost no net azimuthal momentum gain by the electrons, as indicated by point A. On the other hand, the protons (and thus the plasma) can gain considerable (negative) azimuthal momentum, as indicated by point B, which contributes positively to net plasma OAM.

The evolution of the axial OAM of all electrons, protons, and all particles are shown in Fig. 2(f). The particle OAM is calculated from summing $\vec{r} \times \vec{p}_{e,p}$ over all particles and normalized by that (namely, $J_x = E_{L0}/\omega$ [1]) of a pure LP LG₀₁ mode with the same energy E_{L0} as the incident Gaussian laser. In our simulation, $E_{L0} = 0.0141 \text{ J}$ and $J_x = 6.0 \times 10^{-18} \text{ kg m}^2 \text{ s}^{-1}$. The electrons are almost OAM free and the protons can eventually gain considerable negative OAM with magnitude larger than 70%. The LG mode coefficient from mode decomposition and the overall OAM are two parameters describing the detail and the macro characteristics of the output vortex laser. Here we define the laser OAM conversion efficiency as J_L/J_x , where J_L denotes longitudinal OAM of output laser and is calculated by integrating $\epsilon_0 \vec{r} \times (\vec{E} \times \vec{B})$ over all space. J_L can reach a large value of about $4.4 \times 10^{-18} \text{ kg m}^2 \text{ s}^{-1}$ after the modulation and the corresponding OAM conversion efficiency can reach $\sim 73\%$. As expected, compared with plasma particles, a nearly equal amount of OAM, but in the positive direction, is gained by the laser. Note the OAM gained by the laser here is nearly more than twice that of the existing schemes, where the OAM conversion efficiency is about 37% ($J_L = 1.1 \times 10^{-17} \text{ kg m}^2 \text{ s}^{-1}$ and $J_x = 3.0 \times 10^{-17} \text{ kg m}^2 \text{ s}^{-1}$) [24] and 34% ($J_L = 1.3 \times 10^{-18} \text{ kg m}^2 \text{ s}^{-1}$ and $J_x = 3.8 \times 10^{-18} \text{ kg m}^2 \text{ s}^{-1}$) [27].

The oscillations of the total OAM of the electrons and protons during the laser incidence and exit stages in Fig. 2(f) can be roughly explained as follows. In the incidence stage ($t \sim 20T_0$), the laser equiphase surfaces are still nearly planes separated by the laser wavelength. However, due to the nonuniform azimuthal density distribution, the total proton momentum $P_{y,p}$ in the laser polarization direction y in a slice of thickness less than $\lambda/2$ is nonzero, as can be inferred from Fig. 2(d) and is marked by the point D in Fig. 2(f). But after the laser pulse has entered and propagates in the slab, the OAM oscillations tend to cancel since the plane phase surfaces become warped and mixed. As discussed, the protons also gain negative net axial OAM since they are driven by the charge-separation field. However, with completion of the modulation of the laser phase surfaces into a continuous helical structure and the vortex laser pulse, the proton momentum again become coherent and nonzero, as can be inferred from Fig. 2(e). As a result, the oscillations of the total electron and proton OAM also become coherent in the laser exit stage, as can be seen in the region marked by E in Fig. 2(f).

III. DISCUSSION

For a specific desired LG laser with mode index l , the plasma length L increases with the minimum plasma density n_2 for a fixed maximum density $n_1 \equiv 0.1n_c$. However, mode decomposition indicates that the high order mode component increases with L , while the desired l th mode component

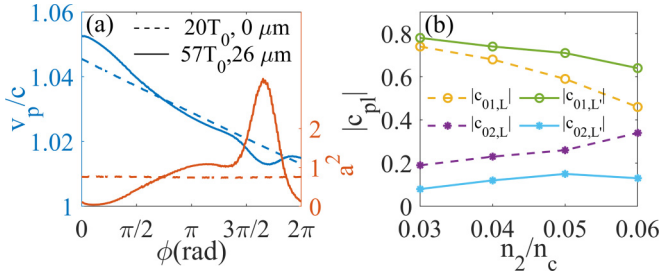


FIG. 3. (a) The dashed curves are for the laser field intensity (orange) and phase velocity (blue) along the circular loop $(r, x) = (2, 0) \mu\text{m}$ at $20T_0$. The solid curves are for the laser field intensity (orange) and phase velocity (blue) along the circular loop $(r, x) = (2, 26) \mu\text{m}$ at $57T_0$. (b) The mode coefficient amplitude versus the minimum plasma density n_2 , with the maximum density n_1 fixed at $0.1n_c$. $C_{01,L}$ and $C_{02,L}$ correspond to LG_{01} and LG_{02} modes in cases with plasma slab length given by L , same for $C_{01,L'}$ and $C_{02,L'}$ while with plasma slab length given by L' .

decreases, as shown by the dashed curves in Fig. 3(b) for $l = 1$ mode generation. This is due to additional v_p modulation from laser energy flow shown in Fig. 3(a). At the very beginning of the laser incidence, the laser intensity a^2 is azimuthally uniform, corresponding azimuthally linear v_p , as represented by the dashed lines. As the laser enters the plasma and be modulated, a^2 redistributes, as given by the solid orange curve [also by the black curve in Fig. 2(b)]. The corresponding v_p is modulated as well, with obvious increase in the $\phi \sim 0^+$ and little decrease in $\phi \sim 2\pi^-$ regions, as shown by the solid blue curve. The synergistical modulation of laser energy flow and v_p is highly nonlinear and theoretical description is difficult. However, we can make a rough analysis by assuming v_p in $\phi \sim 0^+$ region increases linearly with time to $v_p(a_0 = 0) = 1.054c = v_1 + \Delta v$ during the modulation, and $v_p = v_2$ remains unchanged in the $\phi \sim 2\pi^-$ region. In this case the laser phase difference in the $\phi \sim 2\pi^- (0^+)$ regions after modulation by plasma of length L becomes $\Delta\phi(L) = ck[L/v_2 - L/(v_1 + \Delta v/2)] \approx 2\pi l + ckL\Delta v/(2v_1^2) = 2\pi l'$, where $l' = l + ckL\Delta v/(4\pi^2 v_1^2) > l$. Fourier decomposition shows that higher order modes emerge with laser phase of $\exp(-il'\phi)$ with fractional topological charge l' [34]. The higher order modes increase with L , or n_2 , since the $\phi \sim 0^+$ region can catch up with and pass the $\phi \sim 2\pi^-$ region during the modulation, which is also verified in the simulation results shown in Fig. 3(b). Considering the v_p modulation, the modulated plasma length for mode l generation can be approximated by $\Delta\phi(L') = 2\pi l$, with $L' = L(v_1 - v_2)/(v_1 - v_2 + \Delta v/2)$ and L given by Eq. (2). For the modulated plasma length, the mode coefficients are given by the solid curves in Fig. 3(b), where we see that the higher modes are indeed suppressed and the desired $l = 1$ mode dominates. However, the OAM gain of the output vortex laser decreases from 70%–80% for the unmodulated slab length L to 50%–60% for the modulated length L' .

We also found that the azimuthal phase plasma slab is suitable for generating intense circularly polarized vortex laser pulse. Moreover, other vortex modes can be obtained by using suitably phased-density plasma slabs. In addition, with more intense lasers, the overall OAM conversion efficiency remains

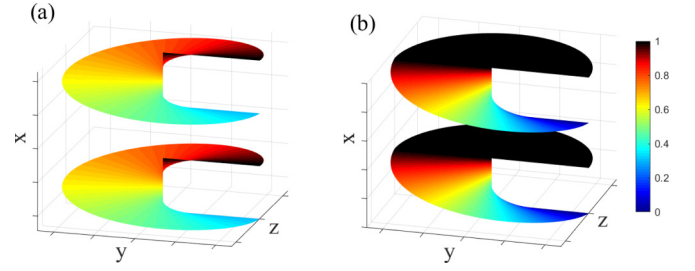


FIG. 4. Evolution of the laser equiphase surfaces during their modulation for (a) the azimuthal plasma phase slab scheme proposed in this paper, (b) the light fan or spiral shaped plasma schemes. The color bar corresponds to the normalized periodic longitudinal displacement of the phase surfaces.

high (60%–70%), but the resulting vortex-beam quality is somewhat degraded: $|c_{01}| = 0.65, 0.59, 0.45$ for $a_0 = 3, 5, 10$ and $n_1 = 0.15n_c, 0.2n_c, 0.35n_c$, and $L = 31, 34, 35 \mu\text{m}$, respectively, for $n_2 = 0.03n_c$, $\Delta t = 10T_0$ and laser focal radius $10 \mu\text{m}$. The laser energy loss is 15%, 22%, and 26%, respectively.

Compared with the light fan, plasma hologram, or spiral shaped plasma, in the present scheme the originally plane laser equiphase surfaces undergo stronger azimuthal modulation, as indicated by Fig. 4(a), which is physically quite different from the other schemes that are indicated by Fig. 4(b). As the input laser enters the plasma slab, its entire ($\phi = 0$ to 2π) equiphase surface is modulated simultaneously to result in different phase velocities, leading to gradual increase of the azimuthal phase gradient, thereby generating azimuthal electromagnetic flux in the entire phase surfaces. In the light fan or spiral shaped plasma schemes, the laser equiphase modulation is indicated by Fig. 4(b), where only the reflected or transmitted parts of the phase surfaces undergo azimuthal modulation, resulting in much less azimuthal electromagnetic flux, since the dark black regions have only longitudinal phase gradient and hence only longitudinal energy flux. The azimuthal energy flux contributes to the longitudinal OAM of the output light, therefore the present scheme with stronger azimuthal electromagnetic energy flow is clearly more efficient with a higher OAM conversion efficiency.

IV. CONCLUSION

In conclusion, a conceptual scheme for vortex beam generation at relativistic intensities involving laser interaction with a uniform-thickness plasma slab of azimuthally varying density is proposed and investigated. The laser-plasma interaction modifies the incident Gaussian laser's plane phase fronts into a continuous helical structure, and laser ponderomotive force and plasma charge separation force impose a torque on the plasma particles, such that the laser light and plasma ions gain oppositely directed axial OAM, with the plasma electrons remaining almost OAM free. Total OAM conversion efficiency for LG_{01} mode realization can reach as high as 73%. Intense vortex lasers are useful for many applications that require light angular momentum at relativistic intensities.

ACKNOWLEDGMENTS

This work was supported by the National Key R&D Program of China (Grant No. 2016YFA0401100); National

Natural Science Foundation of China (NSFC) (Grants No. 11575031, No. 11575298, and No. 11705120); and National ICF Committee in China. K. Jiang acknowledges the support from China Scholarship Council.

-
- [1] L. Allen, M. W. Beijersbergen, R. J. C. Spreeuw, and J. P. Woerdman, *Phys. Rev. A* **45**, 8185 (1992).
- [2] L. Allen and M. J. Padgett, *Opt. Commun.* **184**, 67 (2000).
- [3] S. M. Barnett, *J. Opt. B* **4**, S7 (2001).
- [4] A. M. Yao and M. J. Padgett, *Adv. Opt. Photonics* **3**, 161 (2011).
- [5] K. T. Gahagan and G. A. Swartzlander, *Opt. Lett.* **21**, 827 (1996).
- [6] Y. Zhao, J. S. Edgar, G. D. M. Jeffries, D. McGloin, and D. T. Chiu, *Phys. Rev. Lett.* **99**, 073901 (2007).
- [7] M. Gecevičius, R. Drevinskas, M. Beresna, and P. G. Kazansky, *Appl. Phys. Lett.* **104**, 231110 (2014).
- [8] A. Mair, A. Vaziri, G. Weihs, and A. Zeilinger, *Nature (London)* **412**, 313 (2001).
- [9] D. G. Grier, *Nature (London)* **424**, 810 (2003).
- [10] W. T. Buono, A. Santos, M. R. Maia, L. J. Pereira, D. S. Tasca, K. Dechoum, T. Ruchon, and A. Z. Khoury, *Phys. Rev. A* **101**, 043821 (2020).
- [11] J. Vieira and J. T. Mendonça, *Phys. Rev. Lett.* **112**, 215001 (2014).
- [12] L. B. Ju, C. T. Zhou, K. Jiang, T. W. Huang, H. Zhang, T. X. Cai, J. M. Cao, B. Qiao, and S. C. Ruan, *New J. Phys.* **20**, 063004 (2018).
- [13] C. Baumann and A. Pukhov, *Phys. Plasmas* **25**, 083114 (2018).
- [14] G. Pariente and F. Quéré, *Opt. Lett.* **40**, 2037 (2015).
- [15] X. Zhang, B. Shen, Y. Shi, X. Wang, L. Zhang, W. Wang, J. Xu, L. Yi, and Z. Xu, *Phys. Rev. Lett.* **114**, 173901 (2015).
- [16] A. Denoëud, L. Chopineau, A. Leblanc, and F. Quéré, *Phys. Rev. Lett.* **118**, 033902 (2017).
- [17] Y. Y. Chen, J. X. Li, K. Z. Hatsagortsyan, and C. H. Keitel, *Phys. Rev. Lett.* **121**, 074801 (2018).
- [18] L. B. Ju, C. T. Zhou, T. W. Huang, K. Jiang, C. N. Wu, T. Y. Long, L. Li, H. Zhang, M. Y. Yu, S. C. Ruan *et al.*, *Phys. Rev. Appl.* **12**, 014054 (2019).
- [19] N. R. Heckenberg, R. McDuff, C. P. Smith, H. Rubinsztein-Dunlop, and M. J. Wegener, *Opt. Quantum Electron.* **24**, S951 (1992).
- [20] M. W. Beijersbergen, R. P. C. Coerwinkel, M. Kristensen, and J. P. Woerdman, *Opt. Commun.* **112**, 321 (1994).
- [21] W. Shu, D. Song, Z. Tang, H. Luo, Y. Ke, X. Lü, S. Wen, and D. Fan, *Phys. Rev. A* **85**, 063840 (2012).
- [22] C. Loussert, K. Kushnir, and E. Brasselet, *Appl. Phys. Lett.* **105**, 121108 (2014).
- [23] M. D. Williams, M. M. Coles, D. S. Bradshaw, and D. L. Andrews, *Phys. Rev. A* **89**, 033837 (2014).
- [24] Y. Shi, B. Shen, L. Zhang, X. Zhang, W. Wang, and Z. Xu, *Phys. Rev. Lett.* **112**, 235001 (2014).
- [25] A. Leblanc, A. Denoëud, L. Chopineau, G. Mennerat, P. Martin, and F. Quéré, *Nat. Phys.* **13**, 440 (2017).
- [26] J. Vieira, R. M. G. M. Trines, E. P. Alves, R. A. Fonseca, J. T. Mendonça, R. Bingham, P. Norreys, and L. O. Silva, *Nat. Commun.* **7**, 1 (2016).
- [27] T. Long, C. Zhou, L. Ju, T. Huang, M. Yu, K. Jiang, C. Wu, S. Wu, H. Zhang, B. Qiao *et al.*, *Phys. Rev. Research* **2**, 033145 (2020).
- [28] G. Z. Sun, E. Ott, Y. C. Lee, and P. Guzdar, *Phys. Fluids* **30**, 526 (1987).
- [29] T. D. Arber, K. Bennett, C. S. Brady, A. Lawrence-Douglas, M. G. Ramsay, N. J. Sircombe, P. Gillies, R. G. Evans, H. Schmitz, A. R. Bell *et al.*, *Plasma Phys. Controlled Fusion* **57**, 113001 (2015).
- [30] D. Bauer, P. Mulser, and W. H. Steeb, *Phys. Rev. Lett.* **75**, 4622 (1995).
- [31] T. W. Huang, C. T. Zhou, A. P. L. Robinson, B. Qiao, H. Zhang, S. Z. Wu, H. B. Zhuo, P. A. Norreys, and X. T. He, *Phys. Rev. E* **92**, 053106 (2015).
- [32] H. Sun, Z. Xu, and C. Gao, *Adv. Mater.* **25**, 2554 (2013).
- [33] Y. Jiang, Z. Xu, T. Huang, Y. Liu, F. Guo, J. Xi, W. Gao, and C. Gao, *Adv. Funct. Mater.* **28**, 1707024 (2018).
- [34] M. V. Berry, *J. Opt. A* **6**, 259 (2004).